Photodissociation Dynamics of 2-Bromopropane Using Velocity Map Imaging Technique J. Phys. Chem. A, , 114 (21) (2010) 6188–6193

Photodissociation Dynamics of 2-Bromopropane Using Velocity Map Imaging Technique

Rongshu Zhu, Bifeng Tang,* Xiu Zhang, and Bing Zhang

Department of physics, Xiaogan University, Xiaogan City, Hubei Province, 432100, P. R. China; Environmental Science and Engineering Research Center, Harbin Institute of Technology Shenzhen Graduate School, Shenzhen 518055, China; State Key Laboratory of Magnetic Resonance and Atomic Molecular Physics, Wuhan Institute of Physics and Mathematics, Chinese Academy of Sciences, Wuhan 430071, P. R. China

Received: February 9, 2010; Revised Manuscript Received: April 27, 2010

Photodissociation dynamics of 2-bromopropane in the A band was investigated at several wavelengths between 232 and 267 nm using resonance-enhanced multiphoton ionization technique combined with velocity map ion-imaging detection. The ion images of Br ($^2P_{3/2}$) and Br* ($^2P_{1/2}$) were analyzed to yield corresponding total translational energy and angular distributions. The total translational energy distributions showed that the channel leading to Br carried more internal energy in the 2-C_3H_7 moiety than the channel leading to Br*. The anisotropy parameters of β (Br) were obtained to be between 0.68 and 1.49, and β (Br*) between 0.73 and 1.96, indicating that the Br* product originates from direct excitation of the $^3Q_0$ state and the $^1Q_1 \rightarrow {}^3Q_0$ nonadiabatic transition, and the Br product from direct excitation of the $^1Q_1$ or $^3Q_1$ state and the $^3Q_0 \rightarrow {}^1Q_1$ nonadiabatic transition. The curve crossing probabilities were determined to be increase with the wavelength. As compared with the case of CH_3Br, the two heavier branched CH_3 groups significantly enhance the Br ($^2P_{3/2}$) production from nonadiabatic contribution. The curve crossing from the $^3Q_0$ to the $^1Q_1$ surface is much higher than that of the reverse from the $^1Q_1$ to the $^3Q_0$ surface, which may have resulted from the difference in shape between the potential energy surfaces of the $^3Q_0$ and $^1Q_1$ states. Finally, based on the experimental data, the partial absorption cross sections of the A band for the $^3Q_0$, $^3Q_1$, and $^1Q_1$ states were extracted.

1. Introduction

Photochemistry of alkyl bromides has received extensive attention for decades, because of their potential effect on ozone depletion, and of the fundamental interest in photodissociation dynamics. Photodissociation of alkyl bromides via excitation to the A band (first absorption continuum) produces ground state, Br ($^2P_{3/2}$), and spin−orbit excited state, Br ($^2P_{1/2}$), bromine atoms labeled as Br and Br*, respectively. Bromine atoms are known to be 40 times more efficient than chlorine atoms in breaking down the atmospheric ozone.[1] The atmospheric decay of alkyl bromides depends largely on their photodissociation rates and product channels in the ultraviolet (UV) region. Thus, it is important to determine their photodynamic behavior for assessing their environmental impact. The excited potential energy surfaces (PES) for alkyl bromides are known to exhibit multiple surface crossings. This, together with the spin−orbit interactions, has made the UV photodissociation of alkyl bromides interesting systems for detailed theoretical studies.

As the simplest alkyl bromides, photodissociation of methyl bromide has been the active focus and serves as a paradigm for research into photodissociation processes that occur along a repulsive potential surface of the excited state. The A band of methyl bromide (centered near 200 nm) arises from an $\sigma^* \leftarrow$ n transition localized on the C−Br bond and consists of an overlapping transitions to three excited states, $^3Q_1$, $^3Q_0$, and $^1Q_1$, as denoted by Mulliken.[2] Excitation in the A band leads to rapid C−Br bond breakage due to the repulsive nature of the excited states. The $^3Q_0 \leftarrow N$ transition is polarized parallel to C−Br bond. The $^3Q_0$ state adiabatically correlates with the spin−orbit excited state Br* by direct dissociation and also contributes to the formation of the ground state Br by nonadiabatic transition near the conical intersection of the $^3Q_0$ and $^1Q_1$ surfaces. The other states are correlated with the spin−orbit ground state Br, and the corresponding transitions to these states are polarized perpendicular to the bond axis. Gougousi and co-workers[3] have studied the photodissociation of methyl bromide using ion imaging in the A band between 215 and 250 nm. They extracted the partial absorption cross sections for the $^3Q_1$, $^3Q_0$, and $^1Q_1$ states of the A band by analyzing the kinetic energy distributions and angular distributions of photofragments. Their results indicated that transitions to the $^3Q_0$ and $^1Q_1$ states dominated the absorption cross section and that there was an important contribution to the Br production from curve crossing between the $^3Q_0$ and the $^1Q_1$ states. The C_{3v} symmetry of CH_3Br may evolve to C_s during dissociation resulting from involvement of a slight H_3C-Br bending vibration.[4,5] The $^3Q_1$ and $^1Q_1$ states therefore split into [2A′, 1A″] and [4A′, 2A″] states, respectively, and the $^3Q_0$ state becomes the 3A′ state. The coupling strength between the $^3Q_0$ (3A′) and $^1Q_1$ (4A′) states is enhanced to cause a significant nonadiabatic transition. The curve crossing also induced higher vibrational excitation in the ν_2 umbrella mode of the methyl radical produced by the Br channel rather than in the Br* channel.[3,5]

As compared with methyl bromide, photodissociation dynamics of 2-C_3H_7Br, which can be regarded as an analogue of methyl bromide with two CH_3 groups substituting two hydrogen atoms branched to the β−carbon atom, has been less studied. The influence of substituted branches and massive size on the C−X bond fission has been the main issue.[4,6] In general, the heavier the branches on the β−carbon atom, the more yields the Br ($^2P_{3/2}$) fragment are found. The methyl substituents lying away from the C−Br bond have less impact on the potential energy surface related to the $\sigma^* \leftarrow$ n transition. As shown in Figure 1,

* To whom correspondence should be addressed. E-mail: tangbf@wipm.ac.cn.

10.1021/jp101260d
Published on Web 05/12/2010

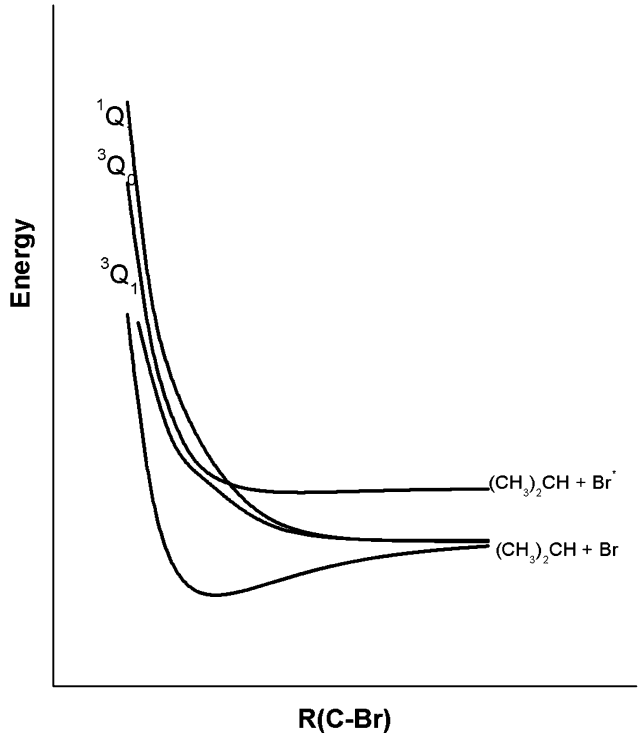

Figure 1. Schematic view of potential energy surfaces involved in 2-C_3H_7Br A band photodissociation.

One-dimensional schematic representation of the potential energy curves involved in 2-C_3H_7Br A band photodissociation is illustrated. Thus, following absorption of an UV photon, these alkyl bromide, 2-bromopropane, dissociates as rapidly as CH_3Br in the regime 80−160 fs.[1] Despite the rapid photodissociation, 2-bromopropane having lower molecular symmetry and heavier branches may show differences in the nonadiabatic transition. Then, the photodissociation of 2-bromopropane is anticipated to yield different behaviors from methyl bromide and is worth to be treated as a model for the substitution effect.

On the other hand, 2-bromopropane is an important substitute for chlorofluorocarbon because it can be easily removed from the troposphere by reaction with OH radical, and is less destructive to the ozone layer than chlorofluorocarbon.[7] Although 2-bromopropane is currently thought to play at most a minor role in stratospheric chemistry, it is still important to know its photochemical properties. The spectroscopy of 2-bromopropane exhibits a broad absorption A band at wavelengths $\lambda <$ 290 nm, with a maximum at about 210 nm.[8] By irradiation at the A band, one can access the direct dissociation of 2-bromopropane. Although other fragmentation routes are possible, the nature of the excited state as well as comparison with analogous halogenated systems[9−14] indicates that the primary reactive step is probably C−Br bond cleavage to leave a nascent 2-propyl radical. Two dissociation channels are possible

$$CH_3CHBrCH_3 \rightarrow CH_3CHCH_3 + Br\,(^2P_{3/2}) \quad \Delta H = 297 \pm 3\ \text{kJ/mol} \quad (1)$$

$$\rightarrow CH_3CHCH_3 + Br\,(^2P_{1/2}) \quad \Delta H = 341 \pm 3\ \text{kJ/mol} \quad (2)$$

In this work, we investigated the photodissociation dynamics of 2-bromopropane in the region from 232 to 267 nm by taking advantage of resonance enhanced multiphoton ionization (REMPI) technique combined with velocity imaging detection. The wavelength dependence of the translational energy distribution and the anisotropy parameter of the photoproducts (Br and Br*) were extracted from the ion image. Given these data, we hoped to reveal detailed dynamical features for the photodissociation of 2-bromopropane in UV range, including the nature of the electronic excited states involved in the photodissociation, the role of nonadiabatic curve crossing in the dissociation, and the effect of substitution of 2 H atoms by methyl groups.

2. Experimental Section

The experimental setup described in detail elsewhere[15] is described here only briefly. The ion velocity imaging apparatus was a modified time-of-flight (TOF) mass spectrometer equipped with an electrostatic ion lens similar to that reported by Eppink and Parker.[16]

The liquid sample of 2-C_3H_7Br was purchased commercially with rated purity 99.9% and used without further purification. The sample seeded in helium at about 1 atm was expanded through a pulsed nozzle with a 0.6 mm orifice into the vacuum. The pulsed nozzle was driven by a valve driver (General Valve, IOTA-1). The molecular beam was skimmed by a 1 mm skimmer mounted ∼6 cm downstream and passed through a hole into the ion lens.

The 355 nm output of an Nd:YAG laser (YG 981 E 10, Quantel) is used to pump a dye laser (Scanmate 2E OG, Lambda Physik), and the output of the dye laser was frequency doubled by a BBO crystal. The linearly polarized UV laser beam is vertically aligned using a Soleil-Babinet compensator, and then focused onto the leading edge of the molecular beam by a lens with a focal length of 200 mm to minimize the effect of cluster formation. The 2-C_3H_7Br molecules are photolyzed by the UV laser light, and the nascent bromine atom fragments are then selectively ionized using the [2 + 1] REMPI technique by the same laser pulse. The expanded bromine ion cloud is projected onto a 2D position-sensitive detector plate that consists of a microchannel plate (MCP) and phosphor screen. To mass select a photofragment, the gain of the MCP was gated by applying a timed voltage pulse (AVRH-3-C, PULSE GENERATOR) on the front plate. Images of the signal on the phosphor screen were recorded using a charge-coupled device (CCD) camera and accumulated in a computer for 30 000 laser shots. During the accumulation of images, the laser wavelength was scanned over a range of $\pm 0.4\ \text{cm}^{-1}$ to cover the Doppler profile of the Br photofragments. The REMPI time-of-flight mass spectra were acquired using a photomultiplier tube instead of CCD camera. The laser, molecular beam, and detection system were run at 10 Hz. Timing was synchronized using a delay pulse generator (Stanford Research System, DG 535).

3. Results

Figure 2 shows the raw images corresponding to Br (a) and Br* (b) generated after the photolysis of 2-bromopropane near 234 nm. Each raw image is a two-dimensional projection of the three-dimensional (3D) speed and angular distributions with cylindrical symmetry around the polarization axis of the photolysis laser. The shape of an image is dependent on the speed and angular distribution patterns of the fragments.

By performing an inverse Abel transformation, a 3D velocity distribution can be reconstructed from a raw image. The raw image was presmoothed, using a Gaussian filter with a 7 × 7 window and a standard deviation of 2 in pixel units, to reduce the noise effect, which may arise during the transformation. The cylindrical symmetry of the velocity distribution allows one to reconstruct a 3D image from every planar slice containing the symmetry axis. The speed distribution can be extracted by

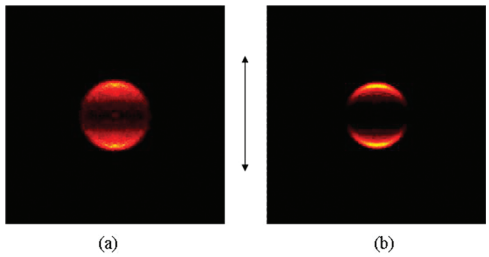

Figure 2. Raw ion images of Br (a) and Br* (b) fragments from the photolysis of 2-bromopropane near 234 nm. The arrow indicates the laser polarization direction.

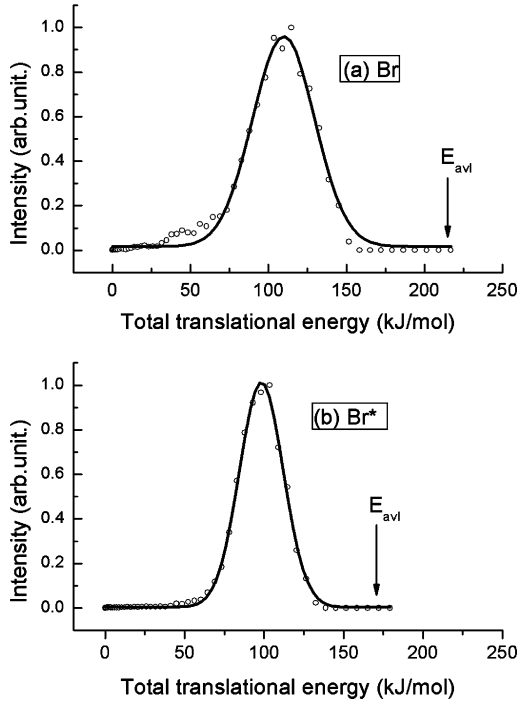

Figure 3. Total translational energy distributions for Br (a) and Br* (b) channels at near 234 nm photolysis wavelength. The solid lines show Gaussian fitting. The arrows indicate the available energies, E_{avl}.

integrating the reconstructed 3D speed distribution over all angles at each speed. The center-of-mass translational energy distribution, $P(E_T)$, is obtained by converting the speed distribution using the equations

$$P(E_T) = P(V)\frac{dV}{dE_T} \tag{3}$$

$$E_T = \frac{1}{2}(m_{Br} + m_{CH_2Cl})\frac{m_{Br}}{m_{CH_2Cl}}V_{Br}^2 \tag{4}$$

The total translational energy distributions $P(E_T)$ for Br and Br* channels are presented in Figure 3, panels a and b, respectively.

The values of f_T in Table 1 designate the fractions of the translational energy. They represent the ratio of the average translational energy, $\langle E_T \rangle$, to the available energy, E_{avl},

$$f_T = \frac{\langle E_T \rangle}{E_{avl}} \tag{5}$$

The available energy is calculated by

$$\begin{aligned} E_{avl} &= h\nu - D_0 - E_{el} + E_{int}^P \\ E_{avl} &= E_T + E_{int} \end{aligned} \tag{6}$$

where $h\nu$ is the photon energy. The C−Br bond dissociation energy, D_0, is 297 ± 3 kJ/mol from the known thermochemical data.[17−19] E_{el} is the electronic energy level of the atomic halogen. A value of 0 kJ/mol is chosen for the ground state Br, and 44.1 kJ/mol[20] for the excited state Br*. E_{int}^P, the internal energy of 2-bromopropane, is estimated to be zero since the rotational and vibrational excitations are negligible in a supersonic molecular beam. E_T is the total translational energy of the photoproducts. E_{int} is the internal energy of 2-C_3H_7, including the rotational and vibrational energy excitations of 2-C_3H_7.

The angular distribution, $P(\theta)$, can be obtained by integrating the reconstructed 3D speed distribution over a proper range of speed at each angle. The anisotropy parameter, β, is extracted by fitting $P(\theta)$ with the standard formula,

$$P(\theta) \propto 1 + \beta P_2(\cos\theta) \tag{7}$$

where θ indicates the angle between the recoil velocity of photofragments and the polarization axis of the photolysis laser. $P(\theta)$ and $P_2(\cos\theta)$ denote the ion signal intensity and the second-order Legendre polynomial, respectively. β varies from 2 (parallel transition) to −1 (perpendicular transition). The observed values are $\beta(Br) = 1.49 \pm 0.06$ and $\beta(Br^*) = 1.94 \pm 0.09$ (Figure 4, panels a and b).

Using the same analysis method, the data for the photodissociation of 2-bromopropane at other wavelengths were also obtained. All data about our results on the photodissociation of 2-bromopropane at each wavelength are listed in Table 1.

4. Analysis and Discussion

Figure 3 shows that the total translational energy distributions of Br and Br* channels can be well fitted by a single-peaked Gaussian curve, implying that Br and Br* are generated as a result of rapid dissociation via repulsive PES after absorbing one UV photon. While comparing these two profiles, we find the Br fragment with a wider distribution, indicating that the Br channel was accompanied by a greater range of internal excitation in the 2-C_3H_7 moiety than the channel leading to Br* + 2-C_3H_7. From Table 1 we can see that the total available energy and the subsequent translational energy for the Br and Br* channels increase with decreasing wavelength. In contrast, the corresponding fractions of the translational energy are evaluated to be about 0.53 and 0.58, respectively, which are independent of the photon energy. The Br channel, with a lower fraction of the average translational energy to the available energy, may carry more internal energy in the 2-C_3H_7 moiety than the Br* channel.

In the case of CH_3Br,[3,5,21] the amount of CH_3 umbrella mode excitation was greater for the channel producing Br than for the channel producing Br*. Hess et al.[22] have attributed this to the difference in slopes between the potential energy surfaces, stating that the steeper $^3Q_0$ state provides less time for the CH_3 photofragment to relax. In the theoretical study of CH_3I, Morokuma and co-workers[23,24] found that C−H bonds are situated at 90° angles with respect to the C−I bond in the $^1Q_1$ state (i.e., a planar CH_3 geometry), and this angle increases to about 104° for the $^3Q_0$ state (i.e., a pyramidal shaped CH_3). Their trajectory calculations showed that it is easier to excite the ν_2 mode when the CH_3 is planar rather than it is pyramidal, and consequently, dissociation on the $^3Q_0$ state generally yields cold CH_3. Furthermore, Morokuma and co-workers also pointed out that in the case of curve crossing, the substantial change in the geometry of the methyl group from pyramidal to planar causes a significant amount of excitation in CH_3 umbrella mode.

This situation also happened in the photodissociation of 2-bromopropane. Our calculations,[14] using the Gaussian 98 program package[25] at UCIS/6-311++G (2d, p) level, showed

TABLE 1: Average Translational Energies, Available Energies, the Fractions of the Translational Energy, the Anisotropy Parameters, and the Intermediate States Involved in the REMPI Detection of Br Atom for Photolysis of *i*-C_3H_7Br in the Wavelength Range of 232−267 nm

channels	λ (nm)	intermediate state	E_{avl} (kJ/mol)	$\langle E_T \rangle$ (kJ/mol)	f_T ($\langle E_T \rangle / E_{avl}$)	β
i-C_3H_7 + Br	232.98	$6p^4P_{1/2}$	216.70	110.64	0.51	1.29 ± 0.05
	233.62	$6p^4P_{3/2}$	215.29	109.71	0.51	1.49 ± 0.06
	250.33	$5p^2S_{1/2}$	181.10	96.46	0.53	1.20 ± 0.06
	252.55	$5p^2P_{3/2}$	176.89	94.48	0.53	0.98 ± 0.05
	254.14	$5p^4S_{3/2}$	173.93	94.02	0.54	0.90 ± 0.05
	260.54	$5p^4D_{3/2}$	162.36	87.83	0.54	0.68 ± 0.05
	266.55	$5p^4P_{3/2}$	152.00	87.89	0.58	0.78 ± 0.05
i-C_3H_7 + Br*	231.87	$5p''^2P_{3/2}$	175.16	99.97	0.57	1.85 ± 0.09
	233.95	$6p^2S_{1/2}$	170.57	98.29	0.58	1.94 ± 0.09
	235.81	$5p'^2P_{1/2}$	166.53	95.81	0.58	1.96 ± 0.08
	238.57	$6p^2P_{1/2}$	160.66	93.17	0.58	1.76 ± 0.08
	239.8	$6p^2P_{3/2}$	158.09	91.24	0.58	1.88 ± 0.08
	266.61	$5p^4S_{3/2}$	107.90	72.412	0.67	0.73 ± 0.04

that for 2-bromopropane the C−C bonds are situated at 109° angles with respect to the C−Br bond in the $^3Q_0$ state, and the angle decreases to about 102 and 91° for the $^3Q_1$ and $^1Q_1$ states, respectively. So, we guess, in the case of curve crossing, from the $^3Q_0$ state to the $^1Q_1$ state or from the $^3Q_0$ state to the $^3Q_1$ state, the substantial change in the geometry of the 2-C_3H_7 moiety would cause a significant amount of excitation in 2-C_3H_7 vibrational modes. This behavior is confirmed by our Br images (as Figure 2a) by noting that the distribution of photofragments at the poles (produced by curve crossing) is noticeably wider than that at the equator (produced by direct dissociation).

2-bromopropane belongs to C_s symmetry, then as already pointed out, the $^3Q_1$ and $^1Q_1$ states split into [2A′, 1A″] and [4A′, 2A″] states, respectively, and the $^3Q_0$ state becomes 3A′ state. The coupling between the $^3Q_0$ (3A′) and $^1Q_1$ (4A′) state induces a nonadiabatic transition.

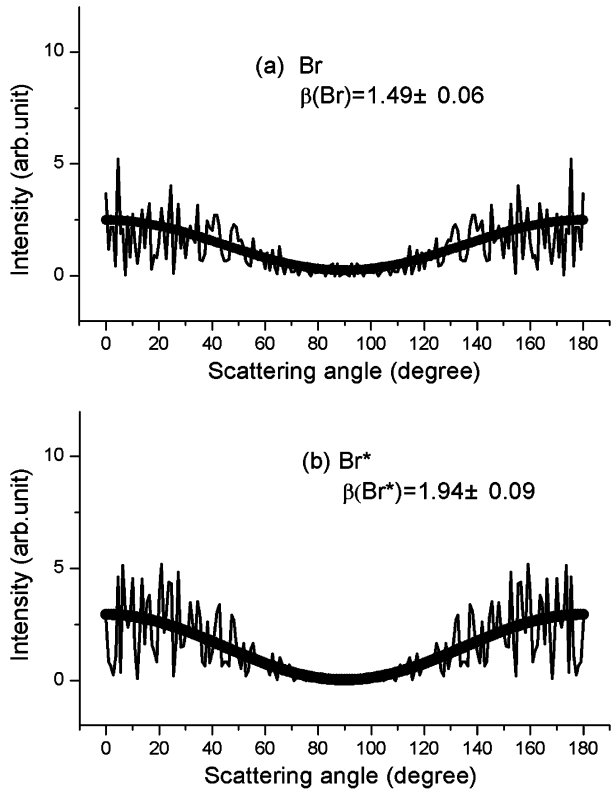

Figure 4. Angular distributions for the Br (a) and Br* (b) fragments at near 234 nm photolysis wavelength.

From Table 1 we can see that the β (Br*) value is β (Br*) = 1.96 ± 0.08 at photolysis wavelength of 235.81 nm, very close to the limit value ($\beta_{//} = 2$) of the parallel transition, suggesting that the Br* product should result substantially from absorption to, and dissociation on, the $^3Q_0$ surface. At the other wavelengths studied, the β(Br*) values are decreased to the range of 1.94 ± 0.09 to 0.73 ± 0.04. This change is caused by both parallel and perpendicular transition contributing into the Br* channel. The Br* product originates from two components: direct excitation of the $^3Q_0$ state and the $^1Q_1 \rightarrow {}^3Q_0$ nonadiabatic transition. The latter contribution increase the perpendicular character ($\beta_\perp = -1$). Whence, classically, the observed β parameter will be a weighted sum of the β parameters for each individual transition. The β(Br) values are between 1.49 ± 0.06 and 0.68 ± 0.05 at each of the wavelengths studied, and again, both parallel and perpendicular transitions are involved into the Br channel. The Br product originates from direct excitation of the $^1Q_1$ or $^3Q_1$ state and the $^3Q_0 \rightarrow {}^1Q_1$ nonadiabatic transition. Therefore, the anisotropy parameters of β(Br) and β(Br*) are related by two factors: the partial absorptions of the $^1Q_1$, $^3Q_0$, and $^3Q_1$ states and the curve crossing probability between the $^3Q_0$ and $^1Q_1$ states. These can be resolved into the relative contributions of the parallel and perpendicular components

$$\beta(\mathrm{Br}) = a\beta_{||} + b\beta_{\perp} \tag{8}$$

$$\beta(Br^*) = c\beta_{||} + d\beta_{\perp} \tag{9}$$

Here, a and b denote the fractions of nonadiabatic transition and direct excitation contributions in the Br product channel, and c and d are the fractions of direct excitation and nonadiabatic transition contributions in the Br* product channel. Provided that β(Br) and β(Br*) are given along with the constraints of $a + b = 1$ and $c + d = 1$, and that the relative quantum yields N(Br) and N(Br*) are determined along with N(Br) + N(Br*) = 1 for normalization, the curve crossing probability between $^3Q_0$ and $^1Q_1$ states is expressed as

$$P_{\mathrm{up}} = \frac{aN(\mathrm{Br})}{cN(\mathrm{Br}^*) + aN(\mathrm{Br})} \tag{10}$$

$$P_{\mathrm{down}} = \frac{dN(\mathrm{Br}^*)}{bN(\mathrm{Br}) + dN(\mathrm{Br}^*)} \tag{11}$$

Here, P_{up} denotes the $^3Q_0 \rightarrow {}^1Q_1$ curve crossing probability, and P_{down} is the $^1Q_1 \rightarrow {}^3Q_0$ curve crossing probability. The

TABLE 2: Curve Crossing Probability, the Relative Quantum Yield, and the Partial Absorptions of the $^1Q_1 + {}^3Q_1$ and $^3Q_0$ States at 234 and 267 nm for *i*-C_3H_7Br; the Curve Crossing Probability and the Relative Quantum Yield at 225 and 245 nm for CH_3Br

molecule	excitation wavelength (nm)	P_{up}	P_{down}	quantum yield Φ(Br*)	$\varepsilon(^1Q_1 + {}^3Q_1)$	$\varepsilon(^3Q_0)$
i-C_3H_7Br	234	0.61	0.06	0.348[a]	0.12	0.88
	267	0.81	0.20	0.196[a]	0.41	0.59
CH_3Br	225	0.20[b]		0.54[b]		
245	0.38[b]		0.46[b]			

[a] Reference 14. [b] Reference 3.

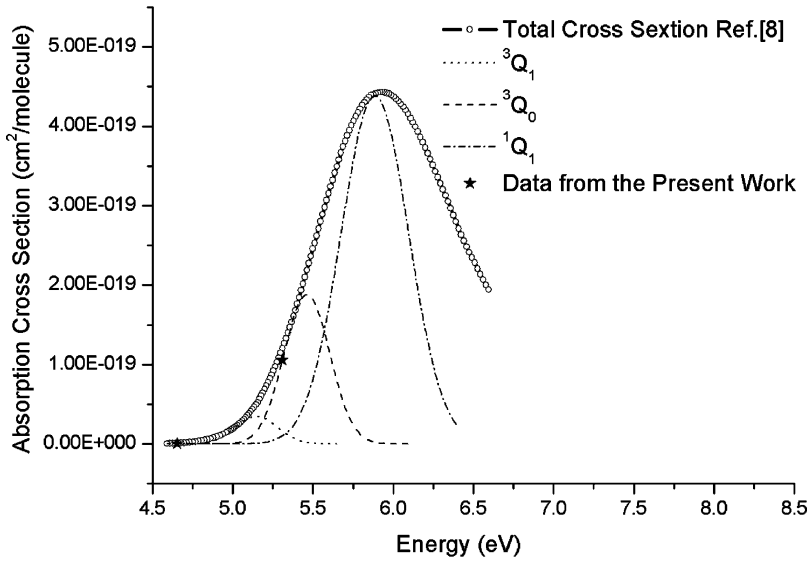

Figure 5. Total and partial absorption cross sections of the A band for 2-bromopropane.

relative partial absorptions of the $^1Q_1 + {}^3Q_1$ and $^3Q_0$ states can be resolved as

$$\varepsilon(^1Q_1 + {}^3Q_1) = bN(\mathrm{Br}) + dN(\mathrm{Br}^*) \quad (12)$$

$$\varepsilon(^3Q_0) = aN(\mathrm{Br}) + cN(\mathrm{Br}^*) \quad (13)$$

Given the measures of β(Br) and β(Br*) from the present work, and the relative quantum yields N(Br) and N(Br*) from ref 14, the curve crossing probability and the relative partial absorptions of the $^1Q_1 + {}^3Q_1$ and $^3Q_0$ states are therefore evaluated to be list in Table 2 at 234 and 267 nm.

In the simple Landau−Zener model, the probability of a curve crossing is proportional to $e^{-c/v}$where c is a constant related to the coupling strength between the states, and v is the fragment velocity at the curve crossing.[5] As shown in Table 2, our results are in agreement with the Landau−Zener model and reveals that the curve crossing probability increase at longer wavelengths is due to decreasing fragment separation velocity.

The curve crossing probability P_{up} and the relative quantum yield at 225 and 245 nm for CH_3Br are also listed in Table 2. Taking into account that there is a blue shift of about 9 nm in the absorption cross section of the A band for CH_3Br relative to that of 2-C_3H_7Br,[3] the data of CH_3Br at 225 nm are comparable with the relevant data of 2-C_3H_7Br at 234 nm. Because there are no data of CH_3Br at 258 nm, we also list the data of CH_3Br at 245 nm compared with the relevant data of 2-C_3H_7Br at 267 nm. From Table 2 we can see, the much higher curve crossing probabilities are found in 2-C_3H_7Br photodissociation. This can also be explained using the Landau−Zener model. The curve crossing probability is anticipated to increase as the two β-branched CH_3 groups become massive and the subsequent separation velocity becomes slower.

From Table 2, we can also see that the probability for the curve crossing from the $^3Q_0$ to the $^1Q_1$ surface is much higher than that of the reverse from the $^1Q_1$ to the $^3Q_0$ surface. If the Landau−Zener model is valid, then the curve crossing probability from the $^3Q_0$ to the $^1Q_1$ surface is the same as its reverse from the $^1Q_1$ to the $^3Q_0$ surface. This disagreement illuminates that the Landau−Zener model holds just for the diatomic molecules, not for the polyatomic molecules, because of its 1D potential surface model, with the reaction coorinate the C−Br bond. In the case of 2-C_3H_7Br, the motion along C−Br bond may induce excitations of the 2-C_3H_7 vibrational modes. As analyzed above, the photodissociation on the $^1Q_1$ surface is associated with more excitations in 2-C_3H_7 vibrational modes than the photodissociation on the $^3Q_0$ surface. So, we say, the $^1Q_1$ surface may be wider than the $^3Q_0$ surface in the dissociation coordinates. We guess the transition from narrow surface to wide surface must be easier than the reverse from wide surface to narrow surface.

The total absorption cross section for 2-C_3H_7Br is presented in Figure 5.[8] Using the relative partial absorptions listed in Table 2 and the total cross section values, we determined the contribution of the $^3Q_0$ state at the two wavelengths studied, and fitting those two points with one Gaussian function, we obtained the whole absorption cross section $E(^3Q_0)$ of the $^3Q_0$ state. Subtracting $E(^3Q_0)$ from the total cross section yields a bimodal shaped distribution that we fit with two Gaussian functions corresponding to $E(^3Q_1)$ and $E(^1Q_1)$ shown in Figure 5. Unfortunately, with only two data points available, our estimation of the partial cross sections is not accurate enough. So, further investigations are needed in order completely elucidate the detailed nature of the absorption cross section.

5. Conclusions

The photodissociation of 2-bromopropane in the wavelength range of 232−267 nm cleaves the C−Br bond, generating bromine atoms of ground state Br and spin−orbit excited state Br*. The total translational energy distributions of Br and Br* channels can be fitted well by a single-peaked Gaussian curve, suggesting that bromine atoms are generated by rapid dissociation via a repulsive potential energy surfaces after absorbing one UV photon. The total translational energy distributions also showed that the Br channel is accompanied by hotter 2-C_3H_7 moiety than the Br* channel, which may result from the difference in shape between the potential energy surfaces of the $^3Q_0$, $^3Q_0$, and $^1Q_1$ state, or from the substantial change in the geometry of the 2-C_3H_7 moiety when curve crossing happens. The analysis of the angular distributions of Br and Br* fragments indicates that both Br and Br* product originate from direct excitation and nonadiabatic transition. The wavelength dependence of the curve crossing probability, as well as the much higher curve crossing probability compared with CH_3Br photodissociation, is in agreement with the Landau−Zener model. However, there is an inconsistency that the probability of the curve crossing from the $^3Q_0$ to the $^1Q_1$ surface is much higher than that of the reverse from the $^1Q_1$ to the $^3Q_0$ surface. This disagreement may be ascribed probably to the fact that the $^1Q_1$ surface is wider than the $^3Q_0$ surface in the dissociation coordinates.

Finally, by analyzing the anisotropy parameters and the relative quantum yields, we are able to extract the partial absorption cross sections fro the $^3Q_0$, $^3Q_1$, and $^1Q_1$ states of the A band.

Acknowledgment. All the authors gratefully acknowledge support from National Natural Science Foundation of China, support from Science Foundation of the Education Department of Hubei Province of China (No. Z20082601), and support from the Public Science and Technology Program of Shenzhen (No. SY200806260026A).

Supporting Information Available: The partial absorption cross sections for the $^3Q_0$, $^3Q_1$, and $^1Q_1$ states of 2-bromopropane in the A band are presented in Table 3. This information is available free of charge via the Internet at: http://pubs.acs.org.

References and Notes

(1) Wofsy, S. C.; McElroy, M. B.; Yung, Y. L. *Geophys. Res. Lett.* **1975**, *2*, 215–218.
(2) Mulliken, R. S. *J. Chem. Phys.* **1940**, *8*, 382–395.
(3) Gougousi, T.; Samartzis, P. C.; Kitsopoulos, T. N. *J. Chem. Phys.* **1998**, *108*, 5742–5746.
(4) Tang, Y.; Lee, W. B.; Hu, Z.; Zhang, B.; Lin, K. C. *J. Chem. Phys.* **2007**, *126*, 064302−064309.
(5) Underwood, J. G.; Powis, I. *Phys. Chem. Chem. Phys.* **2000**, *1*, 747–756.
(6) Kavita, K.; Das, P. K. *J. Phys. Chem. A* **2001**, *105*, 315–318.
(7) Takeuchi, Y.; Ichihara, G.; Kamijima, M. *J. Occup. Health* **1997**, *39*, 179–191.
(8) Kozlov, S. N.; Orkin, V. L.; Huie, R. E.; Kurylo, M. J. *J. Phys. Chem. A* **2003**, *107*, 1333.
(9) Zhang, R.; Ghazal, A. Y.; Liu, Y.; Zhang, Y.; Tang, B.; Zhang, B. *Opt. Commun.* **2009**, *282*, 2169–2173.
(10) Tang, Y.; Lee, W. B.; Zhang, B.; Lin, K. C. *J. Phys. Chem. A* **2008**, *112*, 1421–1429.
(11) Hua, L.; Shen, H.; Hu, C.; Zhang, B. *J. Chem. Phys.* **2008**, *129*, 244308–244314.
(12) Hua, L.; Shen, H.; Zhang, C.; Cao, Z.; Zhang, B. *Chem. Phys. Lett.* **2008**, *460*, 50–54.
(13) Zhang, X. P.; Wei, Z. R.; Tang, Y.; Chao, T. J.; Zhang, B; Lin, K. C. *ChemPhysChem* **2008**, *9*, 1130–1136.
(14) Zhu, R.; Tang, B.; Ji, L.; Tang, Y.; Zhang, S.; Zhang, B. *Chem. Phys. Lett.* **2005**, *405*, 58–62.
(15) Liu, P. J.; Tang, B.; Zhang, B. *Chem. Phys.* **2007**, *454*, 141–148.
(16) Eppink, A. T. J. B.; Parker, D. H. *Rev. Sci. Instrum.* **1997**, *68*, 3477–3484.
(17) Davies, J.; Lacher, J. R.; Park, J. D. *Trans. Faraday Soc.* **1965**, *61*, 2413–2416.
(18) Tsang, W. *Heats of Formation of Organic Free Radicals by Kinetic Methods in Energetics of Organic Free Radicals*; Blackie Academic and Professional: London, 1996; pp 22−58.
(19) Chase, M. W. *J. Phys. Chem. Ref. Data, Monograph* **1998**, *9*, 1–1951.
(20) Arepalli, S.; Presser, N.; Robie, D.; Gordon, R. J. *Chem. Phys. Lett.* **1985**, *117*, 64–66.
(21) Chandler, D. W.; Janssen, M. H. M.; Stolte, S.; Strickland, R. N.; homan, J. W.; Parker, D. H. *J. Phys. Chem.* **1990**, *94*, 4839–4846.
(22) Hess, W. P.; Chandler, D. W.; Thoman, J. W. *Chem. Phys.* **1992**, *163*, 277–286.
(23) Amamatsu, Y.; Yabushita, S.; Morokuma, K. *J. Chem. Phys.* **1996**, *104*, 9783–9794.
(24) Amamatsu, Y.; Morokuma, K.; Yabushita, S. *J. Chem. Phys.* **1991**, *94*, 4858–4876.
(25) Frisch, M. J.; Trucks, G. W.; Schlegel, H. B.; Scuseria, G. E.; Robb, M. A.; Cheeseman, J. R.; Zakrzewski, V. G.; Montgomery, J. A., Jr.; Stratmann, R. E.; Burant, J. C.; Dapprich, S.; Millam, J. M.; Daniels, A. D.; Kudin, K. N.; Strain, M. C.; Farkas, O.; Tomasi, J.; Barone, V.; Cossi, M.; Cammi, R.; Mennucci, B.; Pomelli, C.; Adamo, C.; Clifford, S.; Ochterski, J.; Petersson, G. A.; Ayala, P. Y.; Cui, Q.; Morokuma, K.; Malick, D. K.; Rabuck, A. D.; Raghavachari, K.; Foresman, J. B.; Cioslowski, J.; Ortiz, J. V.; Stefanov, B. B.; Liu, G.; Liashenko, A.; Piskorz, P.; Komaromi, I.; Gomperts, R.; Martin, R. L.; Fox, D. J.; Keith, T.; Al-Laham, M. A.; Peng, C. Y.; Nanayakkara, A.; Gonzalez, C.; Challacombe, M.; Gill, P. M. W.; Johnson, B. G.; Chen, W.; Wong, M. W.; Andres, J. L.; Head-Gordon, M.; Replogle, E. S.; Pople, J. A. *Gaussian 98, revision A.3*; Gaussian, Inc.: Pittsburgh, PA, 1998.

JP101260D